Paper ID ILASS08-13-19

EXPERIMENTAL ANALYSIS ON THE CHARACTERISTICS OF WATER DROPS DURING EVAPORATION ON HIGH-EFFUSIVITY, MICROFINNED SURFACES

Manfredo Guilizzoni*, Giorgio Sotgia°

* Department of Energy, Politecnico di Milano, piazza Leonardo da Vinci, 32 – 20133 Milano
Phone: +39 02 2399 3888, Fax: +39 02 2399 3863, E-mail: manfredo.guilizzoni@polimi.it
° Department of Energy, Politecnico di Milano, piazza Leonardo da Vinci, 32 – 20133 Milano
Phone: +39 02 2399 3850, Fax: +39 02 2399 3863, E-mail: giorgio.sotgia@polimi.it

ABSTRACT
A deep understanding of the behaviour of sprays is of great importance in several fields, both industrial (combustion, heat transfer, spray painting) and medical, and the study of the behaviour of single drops is a fundamental step towards the comprehension of the whole phenomenon. Focusing the attention on spray/surface heat transfer problems, the most interesting aspect is the interaction of sessile and impinging drops on solid surfaces. The description or the prediction of the drop shape parameters (height, contact angle and, in particular, contact area) is a necessary pre-requisite for the thermal analysis, especially when pure evaporation is involved. The present paper refers to an experimental analysis on the shape and behaviour of sessile and impinging water drops on smooth and microfinned surfaces of medium/high effusivity materials, in isothermal condition and during evaporation. Drop shape, contact angle and contact area are characterised as a function of the surface material, microfin geometry and Weber number for impinging drops. Preliminary results about the evaporation transients for sessile drops on aluminium and brass surfaces are presented.

INTRODUCTION

The present paper deals with a research study about the wettability of metallic surfaces of different characteristics and the evaporation transients of water drops on such surfaces. A great number of engineering fields requires a precise knowledge of the interactions between fluids and solids [1]. Among the others, the following can be cited: the design of new materials with desired wettability properties, the enhancement of fire fighting systems [2], the cooling of metallic and ceramic surfaces and of electronic devices [4, 5]. The interest in this field is confirmed by the great number of specialized textbooks [6-9] and papers available in literature [10-20]. At the Department of Energy of the Politecnico di Milano research activities are carried out about the wettability of different solid surfaces and their cooling by means of evaporating drops. The research focus is in particular on the geometrical characteristics and evaporation transients of sessile and impinging water drops on microfinned surfaces. Smooth surfaces are also investigated as a reference term. The research program is mainly experimental, but it involved also a numerical approach, concerning the numerical integration of the equilibrium equation of sessile drops on smooth and corrugated surfaces. Numerical results are in good agreement with experimental ones as described in previous papers [21, 22]. Parametric studies of the most important governing quantities are performed by differing surfaces according to their material and shape. For the part of the research involving heat transfer, the attention is mainly focused on medium and high effusivity metallic materials (aluminium, brass) at different temperatures (in all cases lower than the boiling temperature).

EXPERIMENTAL SET-UP

The experimental set up is depicted in Fig.1, with the exception of the "thermal" components which are shown in higher detail in Fig. 2.

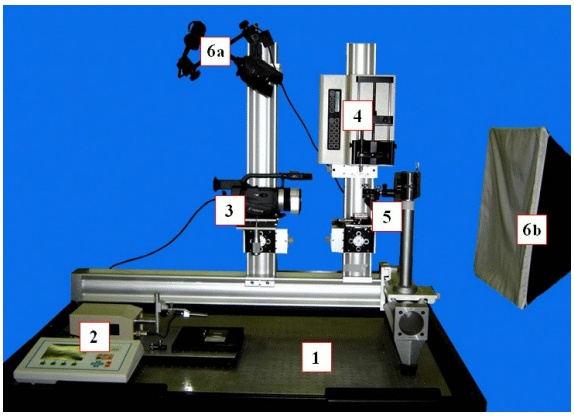

Fig. 1 Experimental set-up: 1) anti-vibrating optical bench; 2) surface analyzer; 3) digital camera; 4) metering pump; 5) surface sample on its support and mirror; 6) lights: concentrated (6a) and diffuse (6b).

The system is located on an anti-vibrating optical bench with a carrying structure in aluminium alloy. A high precision metering pump completed by suitable syringes allows to supply drops of controlled volume on surfaces that can be characterized by means of the surface analyzer (in terms both of profile and of roughness). A lamp equipped with a concentrator and a lamp equipped with a diffuser

provide the lighting necessary to the photographic and video pictures made by a high-resolution digital video/still camera.

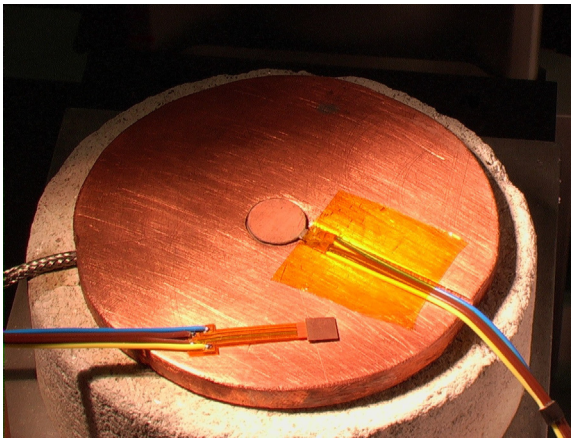

Fig. 2 Thermal part of the experimental set-up: heating and diffusing plates, insulation and thermal fluxmeters.

For the evaporation analysis, an aluminium heating plate regulated by a thermocouple and a PID controller is available, completed by its insulation and by a copper diffusing plate on which the surface sample is positioned. Two thermal fluxmeters, each one including a type-T thermocouple [5], can be used to measure the heat flux (Fig. 2). For the present study, it was mostly used the circular one (diameter 0.01 m) placing it in an appropriate cave in the diffusing plate, centred under the surface sample itself. The cave is filled by means of a mixture of conductive paste (conductivity 7.5 W/mK) and very thin aluminium chips. This is done to increase the conductivity of the cave filling so to reduce the negative effect on the fluxmeter measure which will be described in the following. The system is completed by a personal computer and an electronic acquisition module to sample the signals from the thermocouples and fluxmeters.

EXPERIMENTAL PROCEDURES

The experimental procedures are in part similar between the isothermal (shape and contact area on surfaces at ambient temperature) and the thermal (evaporation transients on hot surfaces) parts of the research activities. First of all, each surface sample is checked by means of the surface analyzer. For “smooth” (surface roughness lower than 0.5 µm) and rough surfaces, the real roughness can be detected; for microfinned surfaces, the geometry, height and regularity of the grooves can be verified, thus reducing the experimental uncertainty due to the differences between the real surfaces and the design ones. This proved to be a very important step because some samples were found not adherent to their design shape [23] or not having a uniform shape, as a consequence of the technological difficulties in realizing micrometer-sized grooves by means of mechanical tools. The surface planarity can be verified too, which is very important to have symmetrical drops without gravity-induced distortions. Figure 3 shows some examples of acquired profiles for eight aluminium and brass microfinned samples, with grooves of different height and spacing. The chemical composition of aluminium and brass samples was checked by means of EDXS-SEM analysis, contemporary getting another confirmation of their shape.

Then, the sample is placed under the syringe. A drop of fixed volume is deposed or let fall from the chosen height on the surface.

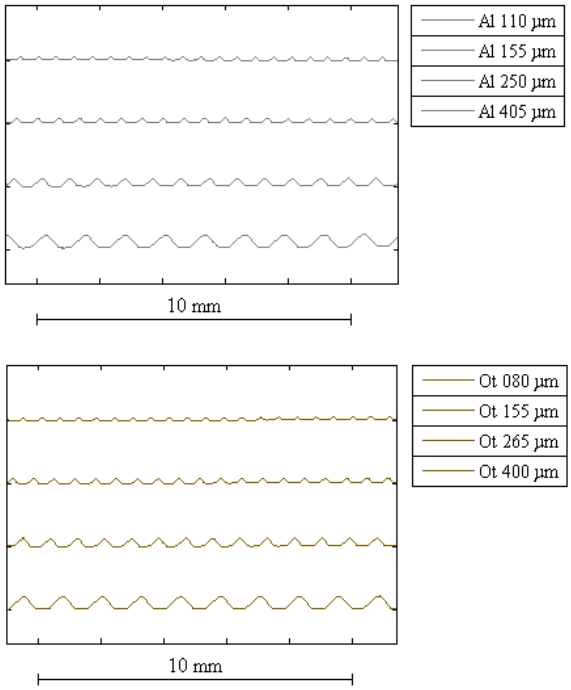

Fig. 3 Profiles of aluminium and brass samples, differing in fin height and spacing, acquired by means of the surface analyzer.

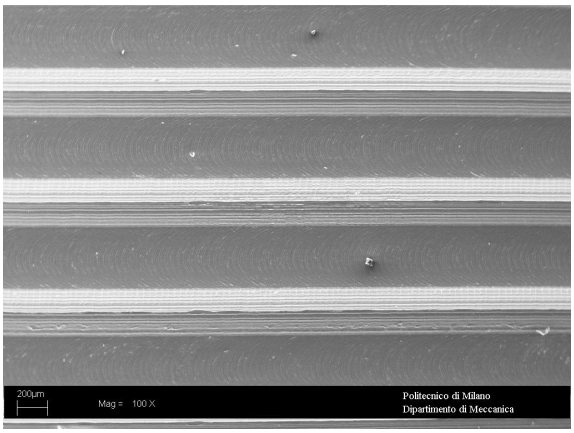

Fig. 4 Aluminium sample (fin height 155 µm) seen using a SEM microscope.

As the drops would detach from the syringe needle with a volume related to the diameter of this last, only small volumes could be obtained for impinging drops. To bypass this limitation, the needle is inserted in a cylindrical hole made in a little Plexiglas® block, so that the liquid is guided to the bottom side of the block and drops detach from a “infinite” flat surface. This enables to obtain bigger drops ($V = 85 \cdot 10^{-9}$ m^3), which are more suitable for the study of microfinned surfaces as they cover more fins. Big drops obtained this way have also disadvantages: they move and deform more than little ones during their detachment and fall, so that it is much more difficult to get a uniform drop distribution. Top and/or side shots or videos of the drop are acquired by means of the videocamera and transferred to the PC. *Ad hoc* software was developed, mostly using the Matlab

programming environment, to process pictures/videos extracting drop contour, contact angle and contact area (both apparent in the case of rough and microfinned surfaces). Figure 5 shows a sequence of pictures which are an example of the extraction of contour and contact angle from a side view and of contact area from a top view.

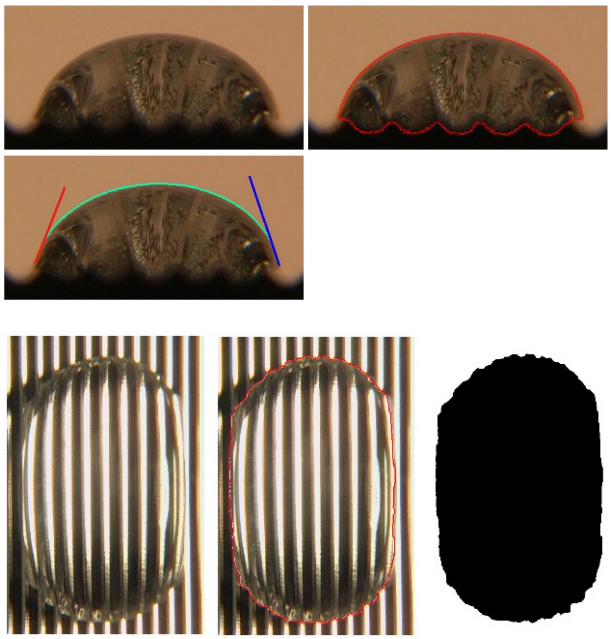

Fig. 5 Contact angle and contact area extraction from side and top views of drops.

The processing of the side pictures can be done mainly automatically, by filtering the difference between an image with the drop and an image of the background only, without the drop. To avoid the disturbance given by the shadow of the drop in the top views, the drop contour and apparent contact area in these pictures have on the contrary to be extracted manually, using aids like for example the shape selection tool of the GIMP® software. Such a procedure can be applied to the single shots taken for the isothermal part of the research but also to frames extracted from videos capturing the drop evaporation. From these videos the evaporation time can be determined and this information can be compared with the one from the thermal fluxmeter, thus getting an higher confidence on the measurement of such a variable. The absolute value of the fluxes measured by the fluxmeter is of minor interest because they are different from the fluxes truly entering the drop. This can be clearly seen in Fig. 6 which shows the results of a numerical simulation performed using a very simplified model of the system (see [18, 19] for much more sophisticated models). Mass transfer from the drop is not considered and evaporation is taken in account only by adequately increasing the convective coefficient with air. Marangoni convection within the drop is neglected too. Such a model cannot therefore give true indications about the situation within the droplet, but it shows evidently how the heat flow tend to avoid the fluxmeter due to the relatively low thermal conductivity of the fluxmeter itself (which is polymeric in the most part) and in particular of the conductive paste. The fluxmeter should be positioned immediately under the drop, but this is obviously not possible, in particular for microfinned surfaces. Nevertheless, even in its present position, the fluxmeter is definitely influenced by the drop on the sample so that it can give a good description of the flux profile during evaporation. First of all confirming the behaviour of constant contact area / constant flux during the most part of the same. It also shows very clearly the beginning of the evaporation (peak in the flux, Fig. 7). On the contrary, it gives a "smoothed" information on the end of the same, because its measured flux is then influenced by the heat capacity of the diffusing plate and of the sample itself. Due to this aspect, the comparison with the videos is very important to have the most reliable indication about the end of the evaporation.

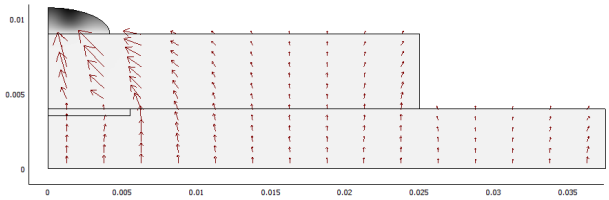

Fig. 6 Temperature (T_{max} = 70 °C, T_{air} = 20 °C) and heat flow distribution in the thermal part of the experimental set-up according to the simplified numerical model.

Figure 7 shows an example of the thermal fluxes acquired by the fluxmeter during the evaporation of V = $85 \cdot 10^{-9}$ m^3 water drops on aluminium samples (Al000 and Al405). The thin lines represent the single acquired flux profiles, while the thick lines indicate their average for the smooth and microfinned surface respectively. The results are presented in dimensionless form by dividing all the fluxes by the mean flux on the dry smooth surface. The flux detected by the fluxmeter for the dry microfinned surface is not significantly different, as it can be clearly seen in the figure.

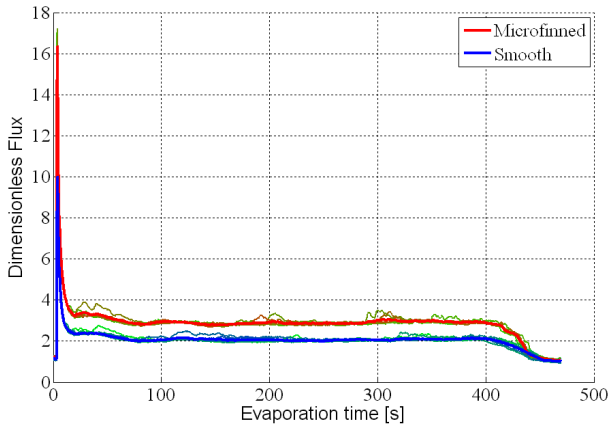

Fig. 7 Examples of dimensionless fluxes acquired by the fluxmeter, showing the beginning, central part and end of the evaporation process.

EXPERIMENTAL CAMPAIGN

The main characteristics of the investigated surfaces are presented in Tab.1, while Tab.2 summarizes the values of the most significant dimensionless groups for the investigated drops. For the campaign described in the present paper, bi-distilled water drops with V = $85 \cdot 10^{-9}$ m^3 were used. The group values are calculated evaluating the thermophysical properties both at 20 °C and 70 °C and referring to an ambient temperature of 20 °C.

Code	Material	H / B / S [µm]	T [°C]
Al 000	Al 97.5% Si 1.0% Mg+Mn+Fe 1.5%	smooth (< 5)	20 / 70
Al 110	Al 97.5% Si 1.0% Mg+Mn+Fe 1.5%	110 / 219 / 575	20 / 70
Al 155	Al 97.5% Si 1.0% Mg+Mn+Fe 1.5%	155 / 291 / 665	20 / 70
Al 250	Al 97.5% Si 1.0% Mg+Mn+Fe 1.5%	248 / 504 / 883	20 / 70
Al 405	Al 97.5% Si 1.0% Mg+Mn+Fe 1.5%	406 / 845 / 1249	20 / 70
Ot 000	Cu 59.5% Zn 40.5%	smooth (< 5)	20 / 70
Ot 080	Cu 59.5% Zn 40.5%	78 / 215 / 582	20 / 70
Ot 155	Cu 59.5% Zn 40.5%	154 / 309 / 665	20 / 70
Ot 265	Cu 59.5% Zn 40.5%	264 / 507 / 867	20 / 70
Ot 400	Cu 59.5% Zn 40.5%	403 / 865 / 1249	20 / 70

Tab. 1 Characteristics of the investigated surfaces.

The microfinned surfaced were designed considering triangular fins with an approximately parabolic increase in the fin height H from one surface to the following: H = 110, 150, 250, 425 µm and corresponding fin spacing S = 575, 665, 875, 1250 µm. The idea was to investigate a broad range of fin heights conserving a major focus on the lower ones. The fin base width B was fixed at 2*H for all the designed surfaces. The technological difficulties in obtaining micrometer-sized grooves on metallic surfaces by means of mechanical tools brought about the real fin geometries indicated in Tab. 1, which were measured using the surface analyzer. Rt and Rz roughness parameters were used as a measure of the fin heights, Fourier transform of the sampled profiles allowed to detect the real fin spacings.

	T = 20 °C	T = 70 °C
Ca	1.04E-1	1.17E-1
Eo	2.60E+0	2.87E+0
Ja	1.30E+1	1.24E+1
Le	8.34E-1	1.09E+0
Ma	1.54E+5	3.45E+5
Pr	7.08E+0	2.55E+0
Ra	1.63E+4	1.03E+5
Re	2.17E+4	1.35E+5
We	0: 5 :80	

Tab. 2 Values of the most significant dimensionless groups for the investigated drops. See [18] and [19] for the definitions of all groups except We.

Impinging drops are classified by means of a modified Weber number. Its expression is rewritten replacing the kinetic energy term with a potential energy one, due to the low value of the fall height which makes air resistance negligible (within a very few percent of the total energy). Air-water buoyancy forces are largely negligible too. Therefore $We = \rho_l \, g \, z \, V_l^{2/3} / \sigma_l$. The investigated We numbers range from 0 (sessile drops) to 80, even if 40 is in general the limit over which the drop breaks at the impact, with formation of secondary drops.

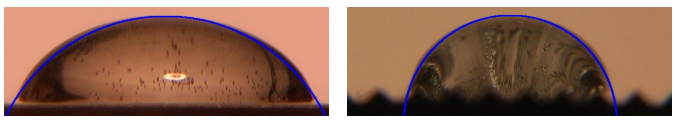

Fig. 8 Deviation from the "circular profile" approximation for two $V = 85 \cdot 10^{-9}$ m³ drops on a smooth (Ot000) and a microfinned (Ot400) surface.

For sessile drops, Fig. 8 shows how the shape of the investigated drops does not fit the "circular profile" approximation during isothermal analysis and at the beginning of the evaporation process, while during this last (which on aluminium and brass happens at constant contact area / variable contact angle confirming literature results) the agreement becomes increasingly better.

RESULTS

The first interesting aspect is the difference in shape between sessile and impinging drops on microfinned surfaces. In the sessile case, there is a very strong "pinning on sharp edges" effect and the drops are very elongated in the direction parallel to the grooves. Along this direction, apparent contact angles are similar to the ones on smooth surfaces. On the contrary, on transversal, cross-fin sections the drop width is much reduced and apparent contact angles are higher than on the corresponding smooth surface, in many cases superior to 90° (Fig. 9).

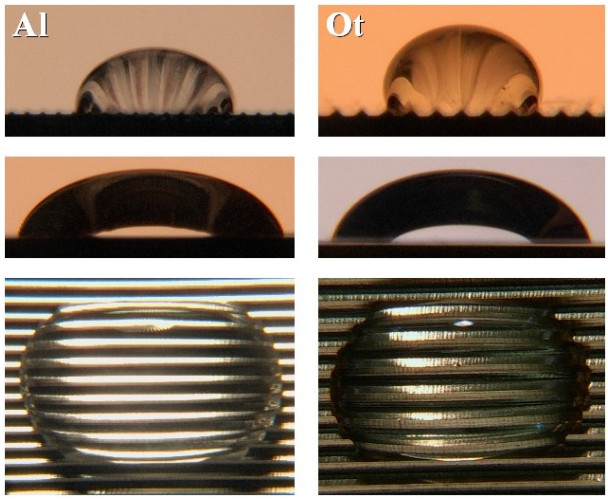

Fig. 9 Front, side and top views of sessile water drops on aluminium (Al155, left side) and brass (Ot155, right side) microfinned surfaces.

In Fig. 10, some top views of sessile and impinging drops on Al155 (first row) and Ot265 (second and third rows) microfinned surfaces are presented. It is evident how the above described effects are not present for impinging drops already at the lower values of We number. Drops are much more circular in shape and the "barrier" effect exerted by the microfins is reversed to the point that in some cases the largest diameter becomes the one in the direction transversal to the grooves. In particular for Ot265 it is also evident the increase in the apparent contact area Ap (the contact area projected on an ideal plane cutting the sample at the contact line) at growing We numbers.

Figs. 11 and 12 present some results in terms of apparent contact area on smooth and microfinned aluminium and brass samples at increasing We numbers from the sessile drops (We = 0) to the limit of secondary drops formation. Fig. 13 shows the results for the Al110 samples alone, evidencing the standard deviation together with the mean values. For ideal microfinned surfaces with triangular fins of the kind shown in Fig. 3, it would be easy to convert the apparent contact area into the real one by means of purely geometrical considerations (assuming that the fluid completely fills the grooves). The increase factor between the

real contact area Ar and the apparent contact area Ap would be:

$$Ar / Ap = 1 - B/S + [(B/S)^2 + 4\,(H/S)^2]^{1/2} \qquad (1)$$

On real, mechanically worked samples it can be on the contrary quite difficult to convert with high precision the apparent contact area into the real one. Therefore, considering that it can be measured with great accuracy and that it seems to be well correlated with the evaporation times (as it will be shown in the Results section), the apparent contact area is in general preferred here as a parameter useful to describe the phenomenon.

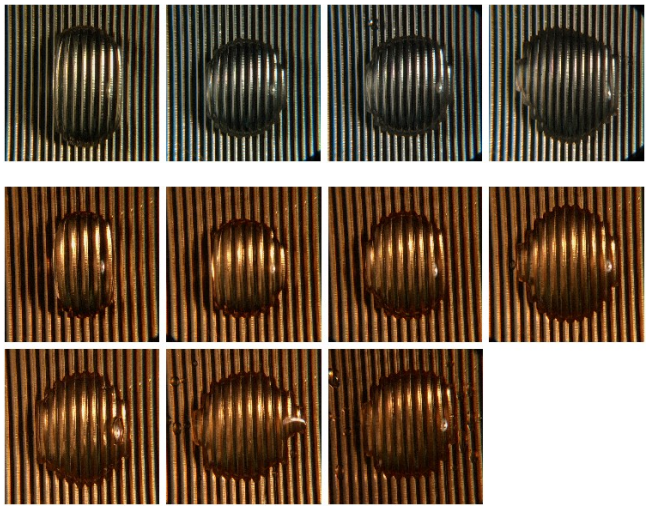

Fig. 10 Sequences of top views of sessile and impinging water drops at increasing We numbers on microfinned surfaces. First sequence (1st row): Al155 - We 0 (Ap 58 mm²), 5 (52 mm²), 10 (57 mm²) and 20 (74 mm²). Second sequence (2nd and 3rd rows): Ot265 - We 0 (Ap 44 mm²), 5 (48 mm²), 10 (60 mm²), 20 (74 mm²), 30 (70 mm²), 40 and 50 (formation of secondary drops).

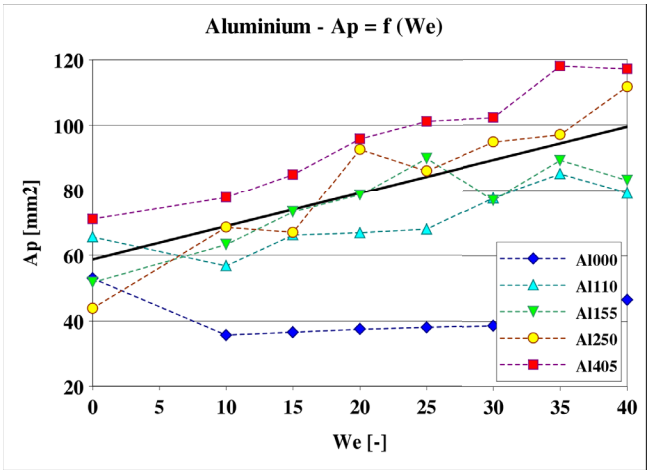

Fig. 11 Apparent contact area for sessile and impinging water drops on aluminium samples of different microfin heights, at increasing We number.

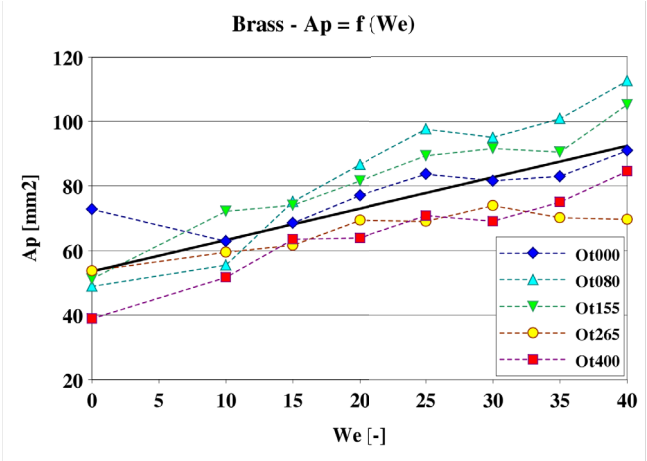

Fig. 12 Apparent contact area for sessile and impinging water drops on brass samples of different microfin heights, at increasing We number.

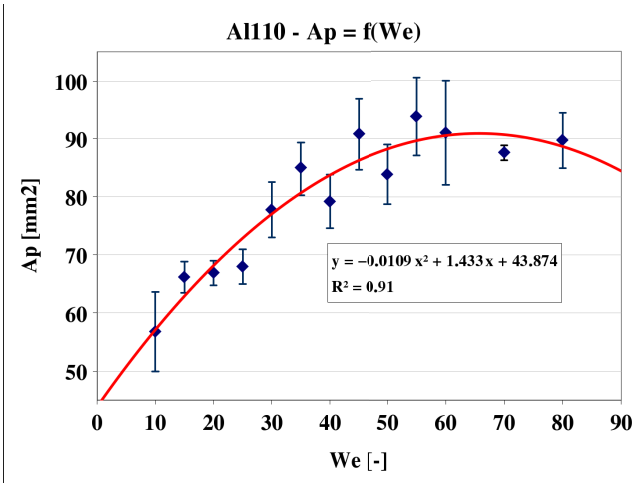

Fig. 13 Mean values and standard deviations of apparent contact area for sessile and impinging water drops on samples of Al110, at increasing We numbers.

Linear and quadratic regression lines are also presented, which give an idea of the general trend of the data even if the dispersion of the same is quite high. For both materials, the apparent contact area increases with We for microfinned surfaces, while on smooth surfaces the behaviour is not monotone from sessile to We drops. In the Al000 case no significant influence of We can be seen. On aluminium, a general trend can also be observed in terms of increase of apparent contact area when increasing the microfin height; while on brass samples the behaviour is more oscillating. In both cases, a wider experimental campaign is without doubt necessary to be able to give more reliable indications. Concerning the experimental activity about evaporation, Figs. 14, 15 and 16 present some processed photographic sequences of drops evaporating on smooth and microfinned surfaces. Fig. 14 shows an evaporating drop on a smooth brass surface (Ot000), at six time steps from the beginning to 300 s. At τ = 360 s, the drop is almost completely evaporated and it would be no longer visible in the picture.

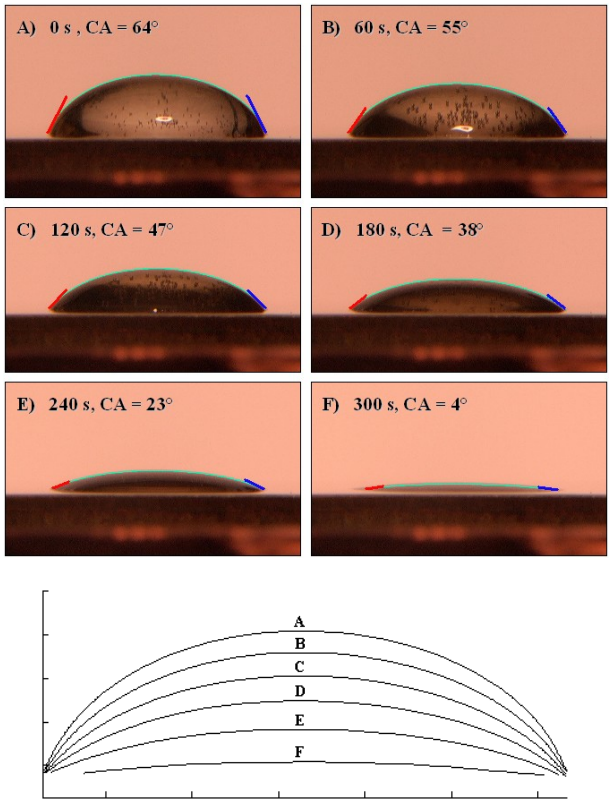

Fig. 14 Evaporation of a V = $85 \cdot 10^{-9}$ m^3 water drop on a smooth brass surface (Ot000) at T = 70 °C: photographic sequence and corresponding contour and contact angle evolution.

All the pictures were processed as previously described and the results in terms of drop contour and contact angles are presented both superposed to the pictures and in the summarizing graph. From both representations, it is also evident the constancy of the drop base width (pinning of the contact line) during the most part of the evaporation. Fig. 15 shows the same analysis for a drop on a microfinned brass surface (Ot400). In this second case too the base width remains constant while the contact angle varies. Fig. 16 shows a sequence of top views of a drop during evaporation on Ot155. The time step is 60 s except that for the last (bottom-right) picture which was taken 450 s after the beginning of evaporation. This is due to the fact that after 480 s the drop was completely evaporated, while in the last picture it can be seen how the drop is by then reduced to a series of fluid stripes within the grooves and it is no longer a unique fluid domain (a situation which could be also observed in Fig. 15H)). This is worth noting because it has the consequence that no single-drop model can be suitable to describe the phenomenon during this last phase of the evaporation. Apart from this aspect, Fig. 16 confirms that the drop width remains constant during evaporation also in the direction parallel to the microfins. On both aluminium and brass, the evaporation proceeds at constant apparent base area / variable apparent contact angle almost until its very end. As a comparison, this is not the case on some polymeric samples, whose results are not presented here, on which the evaporation partially goes on with almost constant contact angle and variable contact area [5]. Another peculiar behaviour that was observed, even if it is not visible in the presented figures, is that the drops completely evaporate firstly on their central part and then on their extremities,

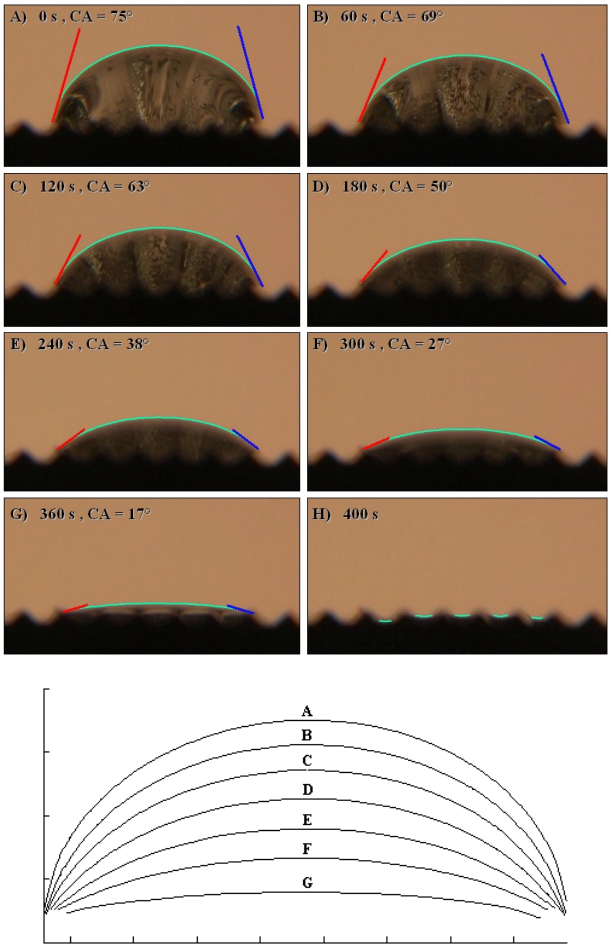

Fig. 15 Evaporation of a V = $85 \cdot 10^{-9}$ m^3 water drop on a microfinned brass surface (Ot400) at T = 70 °C: photographic sequence and corresponding contour and contact angle evolution.

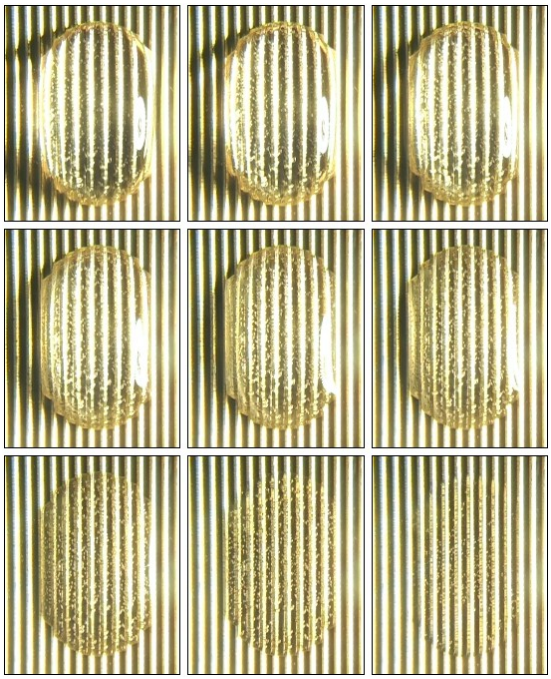

Fig. 16 Evaporation of a V = $85 \cdot 10^{-9}$ m^3 water drop on a microfinned brass surface (Ot155) at T = 70 °C: photographic top-view sequence.

particularly along the grooves direction.

Partly due to the dispersion of the contact areas already observed in the isothermal part of the research activity, a quite high dispersion of the results was observed also in terms of heat fluxes and of evaporation times. Figs. 17, 18 and 19 report some results about the evaporation times of sessile drops on smooth and microfinned aluminium and brass surfaces. For all the presented scenarios at least ten drops were investigated. The box plots in Figs. 17, 18 and 19 are not drawn following Tukey convention: the whiskers ends represent minimum and maximum of the experimental observations, which are often single values quite distant from the others. Due to the fact that the drop volume is the same for all the tests, shorter evaporation times mean higher heat transfer from the surface to the drop and consequently better cooling performances.

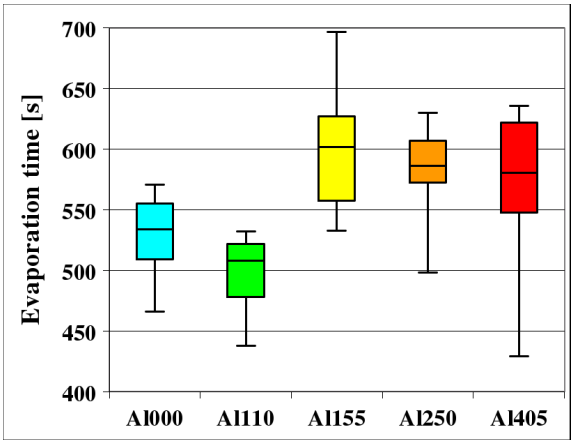

Fig. 17 Evaporation times of V = 85·10^{-9} m^3 sessile water drops on aluminium surfaces.

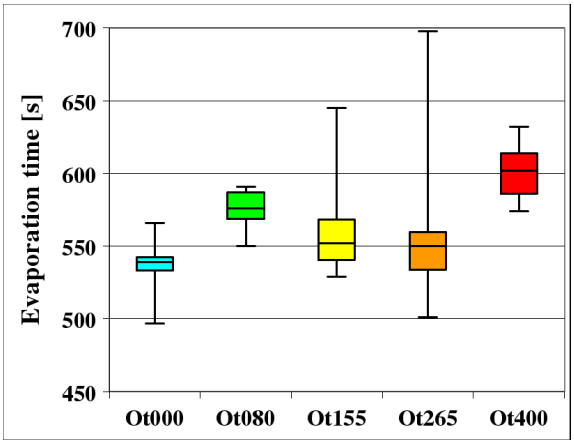

Fig. 18 Evaporation times of V = 85·10^{-9} m^3 sessile water drops on brass surfaces.

Looking at Fig. 19, it is evident how a correlation between the contact areas and the evaporation times is present for brass samples, despite the previously cited dispersion. Real contact areas are calculate using Eq. 1 and the values reported in Tab. 1 for H, B and S. Apparent contact area seems to be better correlated to evaporation times with respect to real contact area, even if a much wider range of data should be acquired to confirm this hypothesis (particularly considering that the behaviour on aluminium surfaces is less regular) and to investigate on its possible causes. In most sessile drop cases, the microfinning decreases the apparent contact area and this results in higher evaporation times. Nevertheless this correlation can be seen as a positive results because impinging drops have in general apparent higher contact areas on microfinned surfaces with respect both to sessile drops on all surfaces and to impinging drops on smooth surfaces. The part of the experimental campaign regarding We drops is at present in progress so that no confirming result can already be presented here.

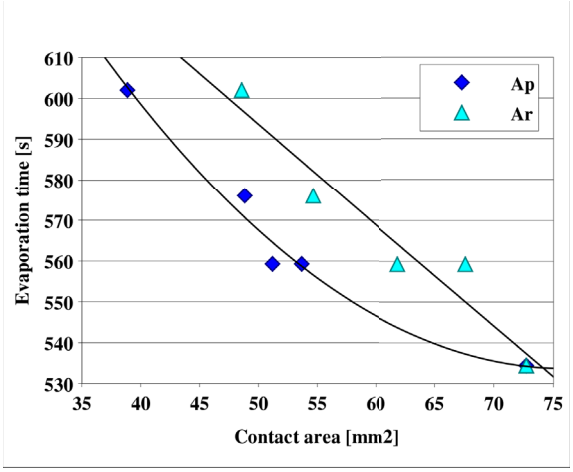

Fig. 19 Evaporation times of V = 85·10^{-9} m^3 sessile water drops on brass surfaces correlated to the real and apparent contact areas.

CONCLUSIONS

An high-quality experimental set-up was built to study the deposition / impact and evaporation of drops on smooth and microfinned surfaces, including a high precision metering pump and a very accurate surface analyzer together with high-level optical bench, videocamera and thermal fluxmeters. Rigorous experimental procedures were developed and tested, which combine video / picture processing and instrumental acquisition and which appears very promising for use in all the many fields where the characterization of drops on surfaces is of interest. Apparent contact area, apparent contact angles and evaporation times can be acquired with accuracy. Results have been presented, referring to water drops on medium / high effusivity metallic (aluminium and brass) surfaces. Both concerning the shape of the drops and their evaporation transients, such results are not completely satisfactory mainly due to their dispersion, which prevents from being able to give reliable prediction about the influence of the microfinning of surfaces on the efficiency of dropwise evaporative cooling. Such dispersion can be related to different causes and further investigation on them is at present being carrying out. Among the most probable causes, there are: the difficulties in obtaining very uniform microfinning on metallic samples by means of mechanical tools (uneven height of the fins, roughness at the bottom of the same); effects of the instabilities and drop movements and deformations during the detachment and the fall for impinging drops. Better mechanical processing would improve the first aspect, while high-speed video acquisition of the drop detachment and fall could help to understand the influence of the second. An extension of the experimental campaign is therefore mandatory before being able to give more reliable indications. Nevertheless, despite their dispersion the obtained results are promising. The

experimental campaign regarding the evaporation of sessile drops confirms a correlation between the drop apparent contact area and its evaporation time (and consequently removed heat flow). It is not a good results for sessile drops, which have a lower apparent contact area on microfinned surface with respect to smooth surfaces, but it is a positive result from a more general point of view. In fact, impinging drops on microfinned surfaces shows higher contact area with respect to sessile drops on all surfaces and to impinging drop on smooth surfaces. If the experimental campaign regarding the evaporation of impinging drops will confirm these results, impinging drops on microfinned surfaces could give significant improvements in the field of dropwise cooling.

ACKNOWLEDGMENT

The authors gratefully thank Barbara Rivolta of the Dipartimento di Meccanica – Politecnico di Milano for performing the EDXS-SEM analysis of the aluminium and brass samples.

NOMENCLATURE

Symbol	Quantity	SI Unit
Ap	Apparent contact area	m^2
Ar	Real contact area	m^2
B	Fin base width	m
CA	(Apparent) contact angle	deg
g	Gravity	$m\,s^{-2}$
H	Fin height	m
S	Fin spacing	m
T	Temperature	°C
V	Volume	m^3
We	Weber number	-
z	Fall height	m
ρ	Density	$kg\,m^{-3}$
σ	Surface tension	$N\,m^{-1}$
τ	Time	s

REFERENCES

[1] P.G. De Gennes, F. Brochard-Wyart, D. Quéré, Capillarity and Wetting Phenomena: Drops, Bubbles, Pearls, Waves, Springer-Verlag, New York, 2005.

[2] S. Chandra, M. Di Marzo, Y. M. Qiao, P. Tartarini, Effect of Liquid-Solid Contact Angle on Droplet Evaporation, *Fire Safety*, Vol. 27, 141-158, 1996.

[3] M. Di Marzo, P. Tartarini, Y. Liao, D. Evans, H. Baum, Evaporative Cooling Due to a Gently Deposited Droplet, *JHMT*, Vol. 36(17), 4133-4139, 1993.

[4] P. Cerisier, L. Grandas, R. Santini, C. Reynard, D. Veyret, L. Tadrist, Etude Experimentale et Numerique des Transferts de Chaleur et de Masse Lors de l'Evaporation d'une Goutte Sessile sur un Support, *12èmes Journées Internationales de Thermique*, Tanger, Maroc, 2005.

[5] L. Grandas, C. Reynard, R. Santini, L. Tadrist, Etude Expérimentale de l'Evaporation, d'une Goutte Posée sur une Plaque Chauffante. Influence de la Mouillabilité, *International Journal of Thermal Sciences*, Vol. 44, 137-146, 2005.

[6] J. Chappuis, G. F. Hewitt, J. M. Delhaye, N. Zuber, Multiphase Science and Technology, McGraw-Hill, New York, 1982.

[7] N. Eustathopoulos, M. G. Nicholas, B. Drevet, Wettability at High Temperatures, Pergamon Material Series, Elsevier Science Ltd., Oxford, 1999.

[8] S. Hartland, R. W. Hartley, Axisymmetric Fluid-Liquid Interfaces, Elsevier, Amsterdam, 1976.

[9] D. Langbein, Capillary Surfaces – Shape, Stability, Dynamics, in particular Under Weightlessness, Springer-Verlag, Berlin, 2002.

[10] J. S. Allen, An Analytical Solution for Determination of Small Contact Angles from Sessil Drops of Arbitrary Size, *Journal of Colloid and Interface Science*, Vol. 261, 481-489, 2003.

[11] C. Bonacina, S. Del Giudice, G. Comini, Dropwise Evaporation, *ASME J. Heat Transfer*, Vol. 101, 441-446, 1979.

[12] G. E. Cossali, A. Coghe, M. Marengo, The Impact of a Single Drop On a Wetted Surface, *Exp. Fluids*, Vol. 22, 463-472, 1997.

[13] G. Cossali, A Fourier Transform Based Data Reduction Method for the Evaluation of the Local Convective Heat Transfer Coefficient, *International Journal of the Heat and Mass Transfer*, Vol. 47, 21-30, 2004.

[14] S. G. Kandlikar, M. E. Steinke, Contact Angle and Interface Behaviour During Rapid Evaporation of Liquid on Heated Surface, *International Journal of the Heat and Mass Transfer*, Vol. 45, 3771-3780, 2002.

[15] Hua Hu, R.G. Larson, Evaporation of a Sessile Droplet on a Substrate, J. Phys. Chem. B, 106 (2002), 1334-1344.

[16] T. S. Meiron, A. Marmur, I. S. Saguy, Contact Angle Measurement on Rough Surfaces, *Journal of Colloid and Interface Science*, Vol. 274, 637-644, 2004.

[17] A. Marmur, Soft Contact: Measurement and Interpretation of Contact Angles, *Soft Matter*, Vol. 2, 12-17, 2006.

[18] R. Mollaret, K. Sefiane, J.R.E. Christy. D. Veyret, Experimental and Numerical Investigation of the Evaporation into Air of a Drop on a Heated Surface, Trans IChemE, Part A, *Chemical Engineering Research and Design*, 2004, 82(A4), 471-480.

[19] O.E. Ruiz, W.Z. Black, Evaporation of Water Droplets Placed on a Heated Horizontal Surface, *ASME Journal of Heat Transfer*, Vol. 124 October 2002, 854-863.

[20] G. Wolansky, A. Marmur, Apparent Contact Angle on Rough Surfaces: the Wenzel Equation Revisited, *Colloids and Surfaces A: Physicochemical and Engineering Aspects*, Elsevier, Vol. 156, 381-388, 1999.

[21] M. Mantegna, G. Sotgia, Theoretical and Experimental Results about Asymmetrical Drops at Rest Upon Surfaces Having Regular Roughness, *ICHMT International Symposium on Heat and Mass Transfer in Sprays Systems*, Antalya, Turkey, 2005.

[22] M. Mantegna, Computation of Asymmetrical Drops at Rest on Surfaces with Regular Roughness According to the Wenzel Equation, *Proc. of. Conf. Two-Phase Flow Modelling and Experimentation*, Pisa, 2004.

[23] Asti L., Guilizzoni M., Sotgia G., Analisi sperimentale sulla forma e sull'area di contatto di gocce sessili ed impattanti su superfici microalettate, *XXV UIT National Heat Transfer Conference*, Trieste, 2007.